

1 **An investigation of Rhinovirus Infection on Cellular Uptake of Poly (glycerol-adipate)**
2 **Nanoparticles**

3

4 Yasmin Abo-zeid^{1,2,3}, Gareth R. Williams², Lila Touabi³, Gary R. McLean^{3,4}

5

6 ¹ Faculty of Pharmacy, Helwan University, Cairo, Egypt

7 ² UCL School of Pharmacy, University College London, 29 – 39 Brunswick Square, London

8 WC1N 1AX, UK

9 ³ Cellular and Molecular Immunology Research Centre, London Metropolitan University, 166-

10 220 Holloway Road, London, N7 8DB, UK

11 ⁴ National Heart and Lung Institute, Imperial College London, Norfolk Place, London W2 1PG

12 UK

13 **Corresponding Author:**

14 Yasmin Abo-zeid^{1, 2, 3}

15 **E-mail:** yasmin.abozeid@pharm.helwan.edu.eg

16 **Mobile:** +201092892746

17

18 **Co-Authors:**

19 Gareth R. Williams²

20 **E-mail:** g.williams@ucl.ac.uk

21 Lila Touabi³

22 **E-mail:** lit0208@my.londonmet.ac.uk

23

24 Gary R. McLean^{3,4}

25 **E-mail:** g.mclean@londonmet.ac.uk

26

27

28 **Abstract:**

29 Viral infections represent 44% of newly emerging infections, and as is shown by the COVID-19
30 outbreak constitute a major risk to human health and wellbeing. Although there are many efficient
31 antiviral agents, they still have drawbacks such as development of virus resistance and
32 accumulation within off-target organs. Encapsulation of antiviral agents into nanoparticles (NPs)
33 has been shown to improve bioavailability, control release, and reduce side effects. However, there
34 is little quantitative understanding of how the uptake of NPs into virally infected cells compares
35 to uninfected cells. In this work, the uptake of fluorescently labeled polymer NPs was investigated
36 in several models of rhinovirus (RV) infected cells. Different multiplicities of RV infections (MOI)
37 and timings of NPs uptake were also investigated. In some cases, RV infection resulted in a
38 significant increase of NPs uptake, but this was not universally noted. For HeLa cells, RV-A16
39 and RV-A01 infection elevated NPs uptake upon increasing the incubation time, whereas at later
40 timepoints (6h) a reduced uptake was noted with RV-A01 infection (owing to decreased cell
41 viability). Beas-2B cells exhibited more complex trends: decreases in NPs uptake (*cf.* uninfected
42 cells) were observed at short incubation times following RV-A01 and RV-A16 infection. At later
43 incubation times (4h), we found a marked decrease of NPs uptake for RV-A01 infected cells but
44 an increase in uptake with RV-A16 infected cells. Where increases in NPs uptake were found, they
45 were very modest compared to results previously reported for a hepatitis C/ Huh7.5 cell line model.
46 An increase in RV dose (MOI) was not associated with any notable change of NPs uptake. We
47 argue that the diverse endocytic pathways among the different cell lines, together with changes in
48 virus nature, size, and entry mechanism are responsible for these differences. These findings
49 suggest that NPs entry into virally infected cells is a complex process, and further work is required

50 to unravel the different factors which govern this. Undertaking this additional research will be
51 crucial to develop potent nanomedicines for the delivery of antiviral agents.

52

53 **Keywords:** Polymer nanoparticles; Poly (glycerol-adipate); virus infection; nanoparticle uptake;
54 HeLa and Beas-2B cells

55

56

57

58 **1- Introduction:**

59 Viral infections represent a public health problem with a major negative impact on health,
60 socioeconomic development and are the biggest pandemic threat in the modern era (Adalja and
61 Inglesby, 2019; Nii-Trebi, 2017). This is clearly evidenced by the 2020 COVID-19 pandemic. All
62 the top priority emerging infectious diseases with the greatest risk of epidemic or pandemic
63 potential are viral diseases (Nii-Trebi, 2017). There are more than 90 antiviral agents in the market
64 (Clercq and E., 2016), but most of them are highly specific to one virus or to members of a viral
65 family and are inactive against other viruses (Adalja and Inglesby, 2019). The high rate of virus
66 mutation, development of antiviral resistance (Irwin et al., 2016), and preponderance of side effects
67 with long term administration of antiviral agents (Chawla et al., 2018) are additional challenges.
68 For example, mitochondrial toxicity recorded with nucleoside reverse transcriptase inhibitors
69 could be lethal (Moyle, 2000). The emergence of new viruses such as SARS-CoV-2 (Pradhan et
70 al., 2020; Zhang et al., 2020) leads to high morbidity rates (Abo-Zeid et al., 2020; Nii-Trebi, 2017;
71 Peters and LeDuc, 1999; Pradhan et al., 2020; Shanks and Brundage, 2012; Zhang et al., 2020)
72 since existing antivirals are often not effective. These challenges require the discovery of new
73 approaches to control virus infections. Broad spectrum antiviral agents are one option; however,
74 there are few of them available for clinical application, and their administration is associated with
75 side effects due to accumulation at off-target organs (such as that observed with ribavirin) (Oventa
76 et al., 2000; Soota and Maliakkal, 2014).

77

78 Nanomedicine could be considered as an alternative strategy to improve the treatment of viral
79 infections. In the scientific literature (Lembo et al., 2018), encapsulation of antiviral agents into
80 nanoparticles (NPs) was found to overcome several limitations of conventional antiviral agents

81 (Szunerits et al., 2015), such as short half-lives and high frequency of drug administration (Harvie
82 et al., 1996) and instability in vivo (Ochekpe et al., 2009). NPs can also improve the delivery of
83 hydrophilic drug into cells (Hillaireau et al., 2006), overcome side effects (Moyle, 2000), improve
84 bioavailability of poorly soluble antiviral agents (Gaur et al., 2014), control/sustain drug release
85 (Lembo et al., 2013), and aid crossing the blood brain barrier (Fiandra et al., 2015); (Nowacek,
86 2010). However, the effect of virus infection on the uptake of NPs has not been studied in detail.
87 To the best of our knowledge, until very recently no studies attempted to quantify NPs uptake by
88 virus infected cells in comparison to un-infected cells. The effect of viral infection on NPs uptake
89 is however an important consideration. NPs are mainly taken up into cells by an endocytic pathway
90 (Foroozandeh and Aziz, 2018) and possibly a down-regulation of endocytosis because of viral
91 infection would make NPs delivery of the appropriate antiviral agent(s) less effective.

92
93 We previously (Abo-zeid et al., 2018b) tracked the uptake of poly(glycerol-adipate) nanoparticles
94 fluorescently labelled with rhodamine B isothiocyanate (RBITC PGA NPs) in human hepatoma
95 cells (Huh7.5 cells) transfected with the hepatitis C virus (HCV) J6/JFH1 chimera (a recombinant
96 HCV designed for maximum replication and virion production *in vitro*). Confocal microscopy
97 demonstrated an enhancement of NPs uptake by infected cells in comparison to non-transfected
98 cells, and by performing flow cytometric analyses, we found that virus transfected cells showed
99 significantly (> 2 times) increased NPs uptake over non-transfected cells. The NPs were not
100 decorated with any ligands to target specific receptors at the surface of Huh7.5 cells. Therefore, a
101 change in cellular physiology due to viral infection was hypothesized to be the driving force
102 responsible for the enhanced NPs uptake.

103

104 In this study, we have investigated if this concept could be further extended to other viruses. We
105 tracked the uptake of RBITC PGA NPs into four models of virus infected cells: (1) HeLa cervical
106 cancer cells infected with rhinovirus A16 (RV- A16), (2) HeLa cells infected with rhinovirus A01
107 (RV-A01), (3) Beas-2B bronchial epithelial cells infected with RV-A16 and (4) Beas-2B cells
108 infected with RV-A01. Non-infected HeLa and Beas-2B cells were employed as controls. These
109 cell lines were chosen because they have diverse biological characteristics and can be infected with
110 RVs. HeLa is a human cervical carcinoma cell line routinely used for the propagation of RVs
111 (Arruda et al., 1997). Beas-2B is a human bronchial epithelial cell line transformed in vitro to grow
112 continuously (Reddel et al., 1988) by infection with SV40 or adenovirus-12 SV40 hybrid virus .
113 Both HeLa and Beas-2B cell lines can be infected with RVs (Bartlett et al., 2012) as they express
114 the major group RV receptor ICAM-1 (Greve et al., 1989) and the minor group RV entry receptor
115 LDLR (Hofer et al., 1994).

116
117 RVs infect the airway epithelium, are considered the most frequent cause of the common cold
118 (Mäkelä et al., 1998). They are also associated with acute exacerbations of asthma and COPD
119 (Johnston et al., 1995; Nicholson et al., 1993; Papi et al., 2006). RVs have further been implicated
120 in acute otitis media, sinusitis, and lower respiratory tract disease (Henquell et al., 2012; Kiang et
121 al., 2007; Winther, 2011). In the current work, RV-A16 and RV-A01 were used as the viruses for
122 study because they are not highly pathogenic (level II pathogens) and represent both the major and
123 minor groups of RVs respectively, entering cells via different entry receptors and endocytic
124 uncoating mechanisms (Schuler et al., 2014). Although both major and minor group RVs enter the
125 endocytic pathway of cells (Fuchs and Blaas, 2009), they are thought to leave endosomes by
126 different mechanisms (Schober et al., 1998). Thus, the use of diverse cells, viruses, entry and

127 uncoating mechanisms should enable us to elucidate if the enhanced uptake of NPs previously
128 reported (Abo-zeid et al., 2018b) with hepatitis C infected Huh7.5 cells is a general phenomenon
129 applicable to all virus infected cells, or whether cell and infection type has an effect on the NPs
130 uptake process.

131

132 **2- Materials and methodology:**

133

134 **2.1. Materials:**

135 Rhinovirus stocks, HeLa and Beas-2b cells were provided by Prof S Johnston, National Heart and
136 Lung Institute, Imperial College London. DMEM medium, RPMI medium, fetal calf serum (FCS),
137 non-essential amino acids (NEAA), anti-human ICAM-1-FITC, penicillin, and streptomycin were
138 supplied by Thermo Fisher. All other materials were purchased from Sigma-Aldrich and used as
139 supplied.

140

141 **2.2. Methodology:**

142 **2.2.1. Synthesis and characterization of poly(glycerol-adipate):**

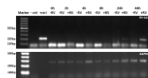
143 The polymer was synthesized following a literature protocol (Abo-zeid et al., 2018a). Briefly,
144 poly(glycerol-adipate) (PGA) was synthesized by dissolving equal amounts (250 mmol) of
145 glycerol and divinyl-adipate (DVA) in dry tetrahydrofuran (THF, 30 ml) in presence of a catalytic
146 enzyme, novozyme 435 (1.25g). The reaction mixture was stirred (overhead stirrer, 200 rpm) at
147 constant temp (50°C) for 24 h. This was followed by enzyme filtration and evaporation of THF to
148 obtain a yellowish jelly-like polymer. This polymer was characterized by gel permeation
149 chromatography (GPC) and ¹H-NMR.

150 GPC were performed following our previous protocol (Abo-zeid et al., 2018a; Kallinteri et al.,
151 2005) using a Polymer Laboratories system, employing 2 mixed bed (D) columns at 40 °C, flow
152 rate 1 ml/min in THF, using an evaporative light scattering detector which was calibrated with 10
153 narrow polystyrene standards. MALDI-TOF data was collected on an Applied Biosystems QSTAR
154 (Q-ToF) mass spectrometer for determination of polymer molecular weight and molecular weight
155 dispersity (\mathcal{D}). Briefly, polymer samples (20 mg) were dissolved in THF (2 ml) and the solutions
156 were mixed for an hour on a roller-mixer (SRT1, Stuart) to allow the polymer to fully dissolve.
157 This was followed by sample filtration using a syringe membrane nylon filter (0.2 μm) before the
158 same was analyzed by size exclusion chromatography and mass spectrometer. $^1\text{H-NMR}$ spectra
159 were recorded on Bruker AVIII HD 400 MHz NMR using a BBFO+ probe and are expressed in
160 parts per million (δ) from internal tetramethylsilane. Polymer and DVA samples were dissolved in
161 acetone- d_6 while glycerol was dissolved in $\text{DMSO-}\text{d}_6$ as previously reported (Abo-zeid et al.,
162 2018a).

163

164 **2.2.2. Preparation and characterization of RBITC PGA NPs:**

165 RBITC PGA NPs were prepared and fluorescent dye loading was optimized as previously reported
166 (Abo-zeid et al., 2018b; Abo-zeid and Garnett, 2020). Briefly, RBITC (200 μl , 1 mg/ml, in
167 methanol) was added into an aqueous phase (HEPES buffer, 10 mM, pH 7.4, 7 ml). The polymer



168 (20 mg) was dissolved in acetone (2 ml) and then added dropwise into the
169 aqueous phase under stirring. The sample was left to stir overnight for complete removal of the
170 organic solvent. RBITC PGA NPs were purified by loading the sample onto a Sephacryl S-200-
171 HR gel column (C2.5 X 40, Pharmacia, bed volume 91 ml). The column was eluted by water using

172 an AKTA prime plus liquid chromatography system (GE Healthcare Life Sciences) at a flow rate
173 of 1 ml/min and collected in fractions of 1.5 ml per tube. The peaks of dye labelled NPs and free
174 dye were detected using a UV detector at 214 nm. The purified NPs dispersion was collected for
175 particle size and zeta potential analysis. Samples were diluted in HEPES buffer (1mM, pH 7.4) to
176 give a count rate ranged between 50 to 300 Kcps and measurements were performed at 25 °C ±
177 0.1 using Malvern Zeta sizer Nano ZS (Malvern Instruments Ltd, Malvern, UK). The dye loading
178 and encapsulation percentages were determined by a direct method, a weighed amount of freeze
179 dried RBITC PGA NPs was extracted in acetone: methanol (1:1 v/v). The fluorescence was
180 measured at $\lambda_{Ex} = 545$ nm and $\lambda_{Em} = 575$ nm using a Hitachi F-4500 spectrofluorometer with
181 slit widths adjusted to 5 nm. The concentration of RBITC was quantified using a pre-determined
182 calibration curve prepared in the same solvent system. Dye loading and dye encapsulation
183 percentages were calculated using Equations 1 and 2 respectively.

184

185
$$\text{Dye loading\%} = \frac{\text{amount of drug (mg)}}{\text{weight of nanoparticles (mg)}} * 100 \quad \text{Equation (1)}$$

186
$$\text{Dye Encapsulation efficacy\%} = \frac{\text{amount of drug entrapped (mg)}}{\text{intial weight added (mg)}} * 100 \quad \text{Equation (2)}$$

187

188 **2.2.3. RVs propagation and tissue culture infectious dose 50% (TCID50) determination:**

189 HeLa cells were grown in T175 flasks in DMEM containing, FCS (10% v/v), penicillin and
190 streptomycin solution (1% v/v). After reaching 80% confluence, cells were used to propagate the
191 virus. The previous medium was removed, and cells were infected with RVs in the presence of
192 DMEM and FCS (2% v/v), penicillin and streptomycin solution (1% v/v). To enhance virus
193 attachment, the flask was gently shaken for 1 h at room temperature. Cultures were incubated for
194 24 h at 37 °C and 5% CO₂ where a cytopathic effect (CPE) greater than 80% was achieved. Cells

195 were then subjected to three freeze-thawing cycles and vortexed briefly to lyse cells and release
196 cell-associated virus. Virus was clarified by centrifugation (4000 rpm, 15 min). Supernatant
197 containing virus was collected, aliquoted and stored at -80°C .

198

199 RV stock solution was titred by infecting a HeLa cell monolayer (1.5×10^4 /well) in a 96 well
200 microtiter plate using a serial diluted virus (10^{-1} to 10^{-9}) in DMEM in presence of FCS (4% v/v),
201 penicillin and streptomycin solution (1% v/v). Plates were incubated at 37°C and 5% CO_2 for 3
202 to 4 days and then wells were scored for presence or absence of CPE by microscopic examination
203 to determine TCID₅₀. The TCID₅₀ refers to the final dilution of RV where there is evidence of
204 infection of 50% of the cultured wells.

205

206 **2.2.4. Cell viability after RV infection:**

207

208 HeLa or Beas-2B cells (4×10^4 /well) were seeded into 24-wells plate. Culture medium [1 ml; either
209 DMEM or RPMI with FCS (10% v/v) and penicillin and streptomycin solution (1% v/v)] was
210 added respectively to HeLa and Beas-2B cells followed by incubation for 24 h at 37°C and 5%
211 CO_2 . Thereafter, the culture media were removed, and cells were treated with virus solutions (1
212 ml) of different multiplicity of infection (MOI): 0.03, 0.3, 0.5, 0.7 and 1. The virus solution
213 comprised RV suspended in DMEM or RPMI in presence of FCS (2% v/v), penicillin and
214 streptomycin solution (1%, v/v). Cells were gently shaken with virus solution for 1 h at room
215 temperature to allow attachment, followed by removal of virus solution and addition of fresh
216 culture medium [1 ml; DMEM or RPMI with FCS (2% v/v) and penicillin/streptomycin solution
217 (1%, v/v)] to the HeLa and Beas-2B cells respectively. Cells were incubated at 37°C and 5% CO_2
218 for 24 h. This was followed by removal of culture medium from all cells and addition of Alamar

219 Blue (AB) solution (1 ml, 36 µg/ml) into each well followed by incubation in the dark at 37 °C and
220 5% CO₂ for 6 h to determine the cells viability. AB solution (36 µg/ml) was prepared by dissolving
221 AB in DMEM or RPMI containing FCS (2% v/v) and penicillin/streptomycin solution (1% v/v)
222 for HeLa cells and Beas2B cells respectively. The fluorescence was measured at excitation and
223 emission wavelengths of 540 and 595 nm respectively using a FLUOstar Omega multi-mode
224 microplate reader (BMG Labtech). Negative (AB solution without cells) and positive (AB solution
225 autoclaved for 15 min) controls were also included in the plate. Two independent experiments
226 were performed where each sample was prepared in triplicate.

227

228 **2.2.5. RV PCR to determine infection:**

229 HeLa cells infected with RV-A16 at MOI 0.5 were placed in a humidified 37 °C incubator at 5%
230 CO₂ and were lysed with RLT buffer (Qiagen) after 2, 4, 8, 24 and 48 h of incubation. RNA was
231 extracted from cells using the RNeasy Mini Kit (Qiagen) following the manufacturer's protocol.
232 Purified RNA samples were reverse transcribed using a RevertAid reverse transcriptase and first
233 strand cDNA synthesis kit (Fisher Scientific) following the manufacturer's instructions. For
234 random hexamer primed synthesis, the reaction mix was incubated for 5 min at 25 °C followed by
235 60 min at 42 °C, and for Oligo (Dt)18 the synthesis reaction mix was incubated for 60 min at 42
236 °C.

237 1µl of cDNA was added to a reaction mix of 49 µl containing PCR buffer, forward and reverse
238 primers (RV-A16 primers were: forward: TATAAAGCTTTCCAAAGGTTGGTCGTG; reverse:
239 TATACTCGAGCTAAGCTAACTGGTGTTTC3'), deoxynucleotide triphosphates dNTPs and Taq
240 polymerase (Fisher Scientific). After an initial denaturing step of 95 °C for 3 min, PCR was run
241 for 40 cycles of 95 °C for 30 s, 52 °C for 30 s, 72 °C for 1 min and a final extension of 72 °C for 5
242 min. Similar conditions were used for amplification of the control gene glyceraldehyde-3-

243 phosphatase dehydrogenase (gapdh) using forward and reverse primers
244 GTCTCCTCTGACTTCAA and ACCACCCTGTTGCTGTA.

245

246 **2.2.6. NPs uptake by cells:**

247 HeLa or Beas-2B cells were seeded into 6-well plates (1.15×10^5 /well), followed by addition of
248 culture medium (2ml) comprising DMEM or RPMI with FCS (10% v/v) and
249 penicillin/streptomycin solution (1% v/v) respectively. The cells were incubated at 37 °C and 5%
250 CO₂ for 24 h. Culture media were removed, and cells were infected with RV at MOI of 0.5 for
251 HeLa cells and MOI of both 0.5 and 1 in the case of Beas-2B cells. Cells were gently shaken with
252 RV for 1 h at room temperature to allow attachment, followed by removal of virus solution and
253 addition of fresh culture medium (2 ml) containing FCS (2% v/v) before the cells were incubated
254 at 37 °C and 5% CO₂ for 24 h. Culture medium was removed and a RBITC PGA NPs colloidal
255 suspension (1.8 ml, 510 µg NPs) added into each well. The colloidal suspension was prepared by
256 adding a purified NPs suspension (850 µl, 510 µg) into an equal volume of FCS, followed by
257 incubation for 24 h. The isotonicity of the NPs suspension was adjusted with phosphate buffered
258 saline (one tablet of PBS was dissolved in 10 ml instead of 100ml to yield 10 times concentrated
259 PBS solution) prior to addition to cells. Cells were incubated for different time intervals. Next, the
260 suspension was removed, and cells were washed with PBS (2 ml, 3 washes). Cell dissociation
261 buffer enzyme-free PBS (0.5 ml) was added to each well and the plate incubated for 10 min to
262 detach cells. The cells were collected and centrifuged (4000 rpm, 15 min). The supernatant was
263 removed, and cells were washed with PBS (2 ml, 3 washes). Cells were then fixed with
264 paraformaldehyde in PBS (1 ml, 2% v/v). A set of non-infected cells were treated similarly but
265 without addition of RV. NPs uptake was tracked using flow cytometry (Guava easyCyte 8HT,

266 MerckMillipore). The settings of the instrument were adjusted as follows: (1) blank cells (HeLa
267 or Beas-2B cells that were not treated with NPs or virus solution) were used to create scatter plots
268 to observe events; (2) non-infected cells (HeLa or Beas-2B cells) previously incubated with
269 RBITC PGA NPs for 6 h were observed by adjusting the setting of the yellow fluorescence
270 channel. Some cells were also stained with anti-human ICAM-1-FITC by incubating on ice for 20
271 min with diluted antibodies followed by PBS washing and fixing with paraformaldehyde in PBS
272 (2% v/v).

273

274 **2.2.7. Statistical analysis:**

275 All statistical analysis was performed using two-way ANOVA followed by a post-hoc Tukey test.

276 Analyses were carried out by GraphPad Prism 8.0 software at confidence level (95%, 99% and

277 99.9%).

278 **3. Results:**

279 **3.1. Synthesis of PGA:**

280 The successful synthesis of PGA was confirmed by ¹H NMR (Figure S1 and S2, Supplementary

281 Information), with the data agreeing with the literature (Abo-zeid et al., 2018a). Size exclusion

282 chromatography analysis gave an estimated Mn of 11.6 kDa, molecular weight dispersity Đ of 1.4,

283 and molecular weight (Mw) of 16 kDa.

284

285 **3.2. Preparation of nanoparticles:**

286 RBITC PGA NPs were prepared by interfacial deposition and fluorescent dye loading was

287 achieved as previously reported (Abo-zeid et al., 2018b; Abo-zeid and Garnett, 2020). The particle

288 size was 110 ± 30 nm (diameter mean \pm SD) and the polydispersity index 0.01, indicating a

289 monodisperse sample. The zeta potential was -53.7 ± 13.3 mv indicating a stable dispersion. The
290 encapsulation efficiency and dye loading were 54 ± 13 % and 0.54 ± 0.13 %, respectively. This
291 dye loading is sufficient enough to track NPs uptake by cells using flow cytometry (Abo-zeid et
292 al., 2018b; Abo-zeid and Garnett, 2020).

293

294 **3.3. Virus infection of cells:**

295 Infection of HeLa cells is used routinely for RV propagation (Arruda et al., 1996) and infection of
296 the human bronchial cell line Beas-2B by RV-A16 and RV-A01 has been shown previously
297 (Bartlett et al., 2012). We made new RV preparations for these studies and demonstrated the
298 TCID₅₀/ml to be 2.96×10^7 for RV-A16 and 3.9×10^7 for RV-A01. To establish conditions of RV
299 infection resulting in minimal cytotoxicity of HeLa and Beas-2B cells and allowing the
300 investigation of NPs uptake into cells, varying multiplicity of infection (MOI) of both RV-A01
301 and RV-A16 was also tested. We found that an increase of MOI was associated with a decrease of
302 cell viability in both HeLa and Beas-2B cells infected with both viruses (Table 1). The viability of
303 HeLa cells was reduced compared to that of Beas-2B cells at higher MOI, and RV-A01 resulted
304 in more cytotoxic effects than RV-A16 in HeLa cells. Only minor effects on the viability of Beas-
305 2B cells were observed with both RV serotypes. For subsequent experiments with NPs, an RV
306 MOI of 0.5 was chosen for HeLa cells and MOI of both 0.5 and 1.0 for Beas-2B cells.

307

308

309

Table 1: Percentage viability of HeLa and Beas-2B cells after RV infection at indicated MOI. Data are shown as mean (standard deviation). Results are average of two independent experiments with three replicates in each

MOI	HeLa cells		Beas-2B cells	
	RV-A16	RV-A01	RV-A16	RV- A01
0.03	99 (4)	100 (6)	106 (5)	108 (7)
0.3	99 (3)	94 (5)	106 (8)	105 (8)
0.5	94 (3)	80 (5)	101 (11)	98 (10)
0.7	90 (5)	73 (8)	101 (6)	99 (9)
1	88 (0)	66 (5)	102 (5)	97 (6)

310

311 To prove RV infection of cells in the absence of sustained cytopathic effects, we performed PCR
 312 to detect the RV genome. Using HeLa cells infected with RV-A16 at MOI of 0.5, RT-PCR was
 313 performed on RNA samples obtained from uninfected and RV-infected cells at several timepoints
 314 (Figure 1). RV-A16 genome was detected in HeLa cells 24 and 48 h after initiation of infection
 315 but not at earlier timepoints. Since the same RV preparations were used to infect Beas-2B cells it
 316 was assumed that MOI of 0.5 and 1 will be sufficient to cause infection, as has been shown
 317 previously (Bartlett et al., 2012).

318

319 **3.4. Nanoparticle uptake by cells:**

320 Having established infection conditions that resulted in infected cells but minimal cytopathic
 321 effects, we next studied the effect of RV infection on the uptake of NPs into cells. We also
 322 investigated expression levels of the RV major group entry receptor intercellular adhesion
 323 molecule-1 (ICAM-1) on infected cells. Figure 2A demonstrates that HeLa cells express ICAM-

324 1, and that expression levels are not altered by RV infection. Incubation with NPs for 6 h resulted
325 in complete uptake of NPs into HeLa cells (lower right quadrant, Figure 2A) that were shown to
326 be ICAM-1 positive (upper right quadrant, Figure 2B). No significant differences in NPs uptake
327 were observed between uninfected and RV-A16 infected cells after incubation with NPs for 6 h
328 (Figure 2B). However, a reduction in NPs uptake by RV-A01 infected cells was noted (Figure 2B).
329 This reduced uptake is most likely due to the lower viability of these infected cells as shown in
330 Table 1.

331
332 Flow cytometry contour plots for the time course analysis of NPs uptake in the absence of ICAM-
333 1 staining are given (Figure 3). The lower left (LL) quadrant represents cells with a low
334 fluorescence signal for RBITC at baseline and shifts to the lower right (LR) quadrant reflect an
335 increase of RBITC fluorescence intensity indicative of NPs uptake. All cells, either infected or
336 non-infected, showed a shift from the LL to LR quadrant with increased incubation times. These
337 data are shown both as percentages of gated cells within the contour plots and as a quantitative
338 number of cells, revealing that similar numbers of events have been analyzed within each condition
339 (Figure 3). The cell numbers appear slightly different because virus infection affects the cells
340 viability, as was discussed earlier in Section 3.3.

341
342 The percentage of positive cells for both uninfected and infected cells increases with the time of
343 incubation with RBITC PGA NPs (Figure 4A), but there is a small reduction within infected cells.
344 Quantitative flow cytometry analysis of NPs uptake in uninfected and infected HeLa cells is
345 presented (Figure 4B) as mean fluorescent intensity (MFI), from which it is apparent that
346 uninfected cells display a comparable MFI to RV-A16 infected cells at 0, 2 and 4h but there is a

347 significant ($P < 0.05$) increase of MFI for RV-A16 cells at 6 h. RV-A01 infected cells demonstrated
348 a significantly ($P < 0.01$) higher MFI than uninfected cells at all timepoints except 6 h, where the
349 MFI was significantly ($P < 0.001$) lower. The latter is matched with the lower percentage of
350 positive cells recorded at 6 h for RV-A01 infected cells.

351
352 Flow cytometry histograms demonstrating the uptake of NPs with time in uninfected and infected
353 Beas-2B cells are depicted in Figure 5A. Both uninfected and infected cells demonstrated an
354 increase in RBITC fluorescence over control cells (cells that were not incubated with NPs, grey
355 filled) at 1 h (red line) and 4 h (blue line) at MOI of both 0.5 and 1. Quantitative flow cytometry
356 plots (Figure 5B) show a similar trend of NPs uptake at MOI of 0.5 and 1. Here, uninfected cells
357 showed a significantly ($P < 0.01$) higher uptake of NPs than infected cells after incubation for 1 h,
358 but upon increasing the incubation time to 4 h RV-A16 infected cells showed significantly higher
359 NPs uptake than uninfected cells ($P < 0.001$ and $P < 0.01$ at MOI of 0.5 and 1 respectively). The
360 opposite was observed with RV-A01 infection, where NPs uptake was significantly lower than
361 uninfected cells ($P < 0.001$ and $P < 0.01$ at MOI of 0.5 and 1).

362

363 **4. Discussion:**

364 Infectious diseases include those caused by bacteria, parasites, fungi and viruses. Virus infections
365 are considered the most challenging due to high rates of virus mutation resulting in new strains
366 that can escape immunity and/or are resistant to antiviral agents, and adverse side effects associated
367 with prolonged administration of antiviral agents. All of these result in reduction in the
368 effectiveness of antiviral therapies. Encapsulation of antiviral agents into NPs has previously been
369 reported to overcome the drawbacks of conventional therapy (Lembo et al., 2018). However, when
370 looking at the literature we could not identify studies investigating the effect of virus infection on

371 the quantitative uptake of NPs. We reported in 2018 (Abo-zeid et al., 2018b) a significant two fold
372 increase of NPs uptake in a HCV-infected liver cell line over that recorded with uninfected cells.

373

374 This study explored four different models of virally infected cells to broaden our understanding
375 into the effect of infection on NPs uptake. We prepared fluorescently labelled RBITC PGA NPs
376 with a dye loading that is sufficient to track the uptake of NPs by flow cytometry (Abo-zeid et al.,
377 2018b; Abo-zeid and Garnett, 2020). These NPs were used for several reasons: they are formulated
378 from PGA, a biodegradable and biocompatible polymer with very low cytotoxic properties (Abo-
379 zeid and Garnett, 2020; Zhang et al., 2014; Kallinteri et al., 2005;), and RBITC is retained in the
380 NPs for a prolonged period of time (Meng et al., 2006), allowing us to track the uptake of NPs
381 rather than free dye (Abo-zeid et al., 2018b). RBITC dye gives a good fluorescence in the acidic
382 pH of lysosomal compartment (Garnett and Baldwin, 1986) leading to effective detection of NPs
383 taken up by cells using flow cytometry (Abo-zeid and Garnett, 2020; Abo-zeid et al., 2018b).

384

385 We confirmed RV infection of cells by RT-PCR and chose two levels of infection (MOI values
386 0.5 and 1) that resulted in infected cells but minimal cytopathic effect to allow the study of virus
387 infection on NPs uptake. Virus infection by RV-A16 and RV-A01 either significantly ($P < 0.05$, P
388 < 0.01 , $P < 0.001$) increased or decreased NPs uptake compared to uninfected cells, depending on
389 the experimental conditions. For HeLa cells, RV-A16 and RV-A01 infection elevated NPs uptake
390 upon increasing the incubation time, but at longer timepoints (6h) a reduced uptake was noted with
391 RV-A01 infection. The latter was likely due to decreased cell viability.

392

393 The picture with Beas-2B cells was more complex, with decreases in NP uptake observed at short
394 incubation times following RV-A01 and RV-A16 infection. An increased incubation time (4h) was
395 associated with a marked decrease of NPs uptake for RV-A01 infected cells but an increase in
396 uptake with RV-A16 infected cells. It can be argued that the reduced HeLa cell viability after
397 infection or viral interference with the mechanism of NPs uptake due to different entry
398 mechanisms of major (RV-A16) and minor (RV-A01) group RVs are responsible for these
399 differences (Fuchs and Blaas, 2012). Furthermore, to observe these changes in NPs uptake, flow
400 cytometric analyses of the MFI was required since no changes in the percentage of cells taking up
401 NPs were seen. However, it is clear that where there is an increased uptake of NPs, this is still
402 relatively minor when compared with our previous study (Abo-zeid et al., 2018b): when Huh7.5
403 cells were transfected with HCV (J6/JFH1 chimera), this resulted in a doubling of NPs uptake.
404 J6/JFH1 is a recombinant HCV generated to maximize replication in cells *in vitro*. It was
405 developed from one HCV variant (JFH1) providing the non-structural components and another
406 strain (J6) providing the structural components to form the intra-genotypic HCV chimera
407 (Lindenbach et al., 2005). It was found that J6/JFH1 chimera has both efficient RNA replication
408 and production of virus particle that could be transfected from culture media of infected Huh7.5
409 cells into naive Huh7.5 cells (Lindenbach et al., 2005).

410

411 The reasons behind the difference in NPs uptake between the cell lines could be both cell-related
412 and virus-related. Firstly, considering cell-related factors, in this study we used HeLa and Beas-
413 2B cells, selected for ease of infection *in vitro* and because they have been used extensively in
414 previous studies. During infection *in vivo*, RVs infect the airway epithelium. However, primary

415 endothelial cell cultures could not be used in this study as the cells are difficult to obtain and
416 maintain *in vitro* for extended periods. Thus, we selected Beas-2B as a suitable alternative.

417

418 The HeLa and Beas-2B cells differ from each other and from the Huh7.5 cells used previously
419 (Abo-zeid et al., 2018b). The main route of NPs uptake into cells is the endocytic pathway
420 (Foroozandeh and Aziz, 2018). A previous study (Sayers et al., 2019) reported differences in the
421 endocytic pathways between cells types, including variations in the endolysosomal morphology,
422 localization, endocytic uptake, trafficking, recycling, endolysosomal pH, the ability of NPs to
423 escape the endosome prior to lysosomal sequestration or exocytosis. These differences have been
424 reported (Sayers et al., 2019) to affect the delivery of mRNA encapsulated into lipid NPs of 120
425 nm, and hence its expression efficiency. We expect that such differences in the endocytic pathway
426 among HeLa, Beas-2B and Huh7.5 cells could cause variations in NPs uptake.

427

428 Virus-related factors will also be important. In our previous study (Abo-zeid et al., 2018b), Huh7.5
429 cells were transfected with a genetically produced chimera virus (JFH1-J6 chimera), while in the
430 current study both HeLa cells and Beas-2B cells were infected with a whole active virus.
431 Additionally, viral structure, size and the entry mechanism into cells could have an effect. RVs are
432 non-enveloped viruses and have a positive-sense single stranded RNA genome that is protected by
433 an icosahedral protein capsid built of 60 copies each of the four viral capsid proteins VP1–VP4
434 (Stobart et al., 2017). In contrast, Hepatitis C virus (HCV) is an enveloped (E1-E2 glycoprotein
435 envelope) positive-sense single stranded RNA virus (Dustin et al., 2016). The particle size of RVs
436 is around 30 nm (Fuchs and Blaas, 2012) and HCV particle size is slightly larger, ranging from 40
437 to 80 nm (Calattini et al., 2015; Gastaminza et al., 2010).

438 RVs we have used here have different mechanisms of entry into cells, as revealed in Figure 6. RV-
439 A16 belongs to the major group of RVs and accesses the host cell by binding to ICAM-1 receptors,
440 while RV-A01 belongs to the minor group and binds to the low density lipoprotein receptor
441 (LDLR) at the surface of the host cell (Fuchs and Blaas, 2012). These events are followed by
442 clathrin mediated endocytosis, resulting in virion uncoating in the early endosome and late
443 endosome for RV-A16 and RV- A01 respectively. This is followed by release of the RV genome
444 into the cytosol for replication and production (Grove and Marsh, 2011). In contrast, HCV entry
445 requires binding to four receptors: CD81, SR-B1, Claudin-1, and Occludin (Pileri et al., 1998);
446 (Scarselli et al., 2002). Once bound to the cell, HCV is sorted by clathrin mediated endocytosis
447 and membrane fusion in the early endosome, followed by virus uncoating and release of genetic
448 material into the cytosol at the late endosome stage (Grove and Marsh, 2011). Virus infection
449 might therefore affect the rate of endocytic pathway uptake of NPs, resulting in either upregulation
450 or downregulation (or potentially have no effect). Consequently, effort should be devoted in the
451 future to study the effect of virus infection on the endocytic pathways to understand how (or if)
452 infection regulates the endocytic uptake of NPs.

453

454 Taken together, we hypothesis that differences in cell types, virus nature, virus size and virus entry
455 mechanism will affect the physiology of the cell and hence have critical effects on the endocytic
456 uptake of NPs. Therefore, future studies should be performed to elucidate the correlation between
457 these factors and the uptake of NPs. Additionally, research modulating the physicochemical
458 properties of NPs (material, morphology, size, zeta potential) and surface decoration (e.g. presence
459 of ligands for active targeting of endocytic receptors of virus infected cells) to identify the key
460 properties controlling their uptake into virus infected cells. Finally, the specific entry receptors

461 expressed at the surface of virus infected cells should be considered, since these could be
462 selectively targeted to assist with the future design of NPs for selective delivery of antiviral agents.

463

464 **4. Conclusions:**

465

466 This work involved development of four models of virus infected cells to probe the effect of virus
467 infection on NPs uptake. It was demonstrated that virus infection in some instances caused a
468 significant increase of NPs uptake compared to uninfected cells. For HeLa cells, RV-A16 and RV-
469 A01 infection elevated NPs uptake upon increasing the incubation time, but at longer timepoints
470 (6h) a reduced uptake was noted with RV-A01 infection (owing perhaps to decreased cell
471 viability). With Beas-2B cells more complex trends are noted, with decreases in NPs uptake (*cf.*
472 uninfected cells) observed at short incubation times following RV-A01 and RV-A16 infection.
473 However, an increased incubation time (4h) was associated with a marked decrease of NPs uptake
474 for RV-A01 infected cells while it led an increase in uptake with RV-A16 infected cells. Where
475 increases in NPs uptake were found, they were very modest compared to results previously
476 reported for a hepatitis C/ Huh7.5 cell line model. We argue that the diverse endocytic pathways
477 among the different cell lines, together with changes in virus nature, size, and entry mechanism
478 are responsible for these differences. This work raises several questions regarding the application
479 of nanomedicine to improve antiviral therapy. To design potent medicines, it will be necessary to
480 understand how virus entry mechanism affects the endocytic pathway of cells, and whether this
481 can modify the uptake of NPs. Further, the subcellular signals of the endocytic pathway affected
482 following virus infection need to be elucidated, and there is an open question as to whether virus
483 infection affects the exocytosis of NPs. Identification of receptors specifically expressed at the

484 surface of virus infected cells could permit the design of NPs to target infected cells, as could
485 greater understanding of how the physicochemical properties of NPs influence uptake.

486

487 **Declaration of interest**

488

489 The authors declare no conflicts of interest.

490

491 **Acknowledgment**

492

493 We would like to thank the British Council and Science and Technology Development Fund in
494 Egypt for awarding a Newton-Mosharafa Researcher Links Travel Grant to Dr. Yasmin Abo-zeid.

495

496 **References**

497 Abo-zeid, Y., Garnett, M.C., 2020. Polymer nanoparticle as a delivery system for ribavirin: Do nanoparticle avoid
498 uptake by Red Blood Cells? *J. Drug Deliv. Sci. Technol.* 56, 101552.

499 <https://doi.org/10.1016/j.jddst.2020.101552>

500 Abo-Zeid, Y., Ismail, N.S., McLean, G.R., Hamdy, N.M., 2020. A Molecular Docking Study Repurposes FDA

501 Approved Iron Oxide Nanoparticles to Treat and Control COVID-19 Infection. *Eur. J. Pharm. Sci.* 153,

502 105465. <https://doi.org/10.1016/j.ejps.2020.105465>

503 Abo-zeid, Y., Mantovani, G., Irving, W.L., Garnett, M.C., 2018a. Synthesis of nucleoside-boronic esters

504 hydrophobic pro-drugs: A possible route to improve hydrophilic nucleoside drug loading into polymer

505 nanoparticles. *J. Drug Deliv. Sci. Technol.* 46, 354–364. <https://doi.org/10.1016/j.jddst.2018.05.027>

506 Abo-zeid, Y., Urbanowicz, R.A., Thomsonb, B.J., William L. Irvingb, A.W.T., Garnett, M.C., 2018b. Enhanced

507 nanoparticle uptake into virus infected cells: Could nanoparticles be useful in antiviral therapy? *Int. J. Pharm.*

508 547, 572–581. <https://doi.org/10.1016/j.ijpharm.2018.06.027>

509 Adalja, A., Inglesby, T., 2019. Broad-Spectrum Antiviral Agents: A Crucial Pandemic Tool. *Expert Rev. Anti.*
510 *Infect. Ther.* 17, 467–470. <https://doi.org/10.1080/14787210.2019.1635009>

511 Arruda, E., Crump, C.E., Rollins, B.S., Ohlin, A.N.N., Hayden, F.G., 1996. Comparative Susceptibilities of Human
512 Embryonic Fibroblasts and HeLa Cells for Isolation of Human Rhinoviruses. *J. Clin. Microbiol.* 34, 1277–
513 1279.

514 Arruda, E., Pitkäranta, A., Witek, T.J., Doyle, C.A., Hayden, F.G., 1997. Frequency and natural history of rhinovirus
515 infections in adults during autumn. *J. Clin. Microbiol.* 35, 2864–2868. [https://doi.org/10.1128/jcm.35.11.2864-](https://doi.org/10.1128/jcm.35.11.2864-2868.1997)
516 2868.1997

517 Bartlett, N.W., Slater, L., Glanville, N., Haas, J.J., Caramori, G., Casolari, P., Clarke, D.L., Message, S.D.,
518 Aniscenko, J., Keadze, T., Zhu, J., Mallia, P., Mizgerd, J.P., Belvisi, M., Papi, A., Kotenko, S. V, Johnston,
519 S.L., Edwards, M.R., 2012. Defining critical roles for NF- κ B p65 and type I interferon in innate immunity to
520 rhinovirus. *EMBO Mol. Med.* 4, 1244–1260. <https://doi.org/10.1002/emmm.201201650>

521 Calattini, S., Fusil, F., Mancip, J., Dao Thi, V.L., Granier, C., Gadot, N., Scoazec, J.Y., Zeisel, M.B., Baumert, T.F.,
522 Lavillette, D., Dreux, M., Cosset, F.L., 2015. Functional and biochemical characterization of hepatitis C virus
523 (HCV) particles produced in a humanized liver mouse model. *J. Biol. Chem.* 290, 23173–23187.
524 <https://doi.org/10.1074/jbc.M115.662999>

525 Chawla, A., Wang, C., Patton, C., Murray, M., Puneekar, Y., Ruitter, A. de C.S., 2018. A Review of Long-Term
526 Toxicity of Antiretroviral Treatment Regimens and Implications for an Aging Population. *Infect. Dis. Ther.* 7,
527 183–195. <https://doi.org/10.1007/s40121-018-0201-6>

528 Clercq, E. de, E., D.C., 2016. Approved antiviral drugs over the past 50 years. *Clin. Microbiol. Rev.* 29, 695–747.
529 <https://doi.org/10.1128/CMR.00102-15.Address>

530 Dustin, L.B., Bartolini, B., Capobianchi, M.R., Pistello, M., 2016. Hepatitis C virus: life cycle in cells, infection and
531 host response, and analysis of molecular markers influencing the outcome of infection and response to
532 therapy. *Clin. Microbiol. Infect.* 22, 826–832. <https://doi.org/10.1016/j.cmi.2016.08.025>

533 Fiandra, L., Colombo, M., Mazzucchelli, S., Truffi, M., Santini, B., Allevi, R., Nebuloni, M., Capetti, A., Rizzardini,
534 G., Prosperi, D., Corsi, F., 2015. Nanoformulation of antiretroviral drugs enhances their penetration across the
535 blood brain barrier in mice. *Nanomedicine Nanotechnology, Biol. Med.* 11, 1387–1397.
536 <https://doi.org/10.1016/j.nano.2015.03.009>

537 Foroozandeh, P., Aziz, A.A., 2018. Insight into Cellular Uptake and Intracellular Trafficking of Nanoparticles.
538 *Nanoscale Res. Lett.* 13, 339–341.

539 Fuchs, R., Blaas, D., 2012. Productive entry pathways of human rhinoviruses. *Adv. Virol.* 2012.
540 <https://doi.org/10.1155/2012/826301>

541 Fuchs, R., Blaas, D., 2009. The enigma of yellow fever in East Africa. *Rev. Med. Virol.* 19, 57–64.
542 <https://doi.org/10.1002/rmv>

543 Garnett, M.C., Baldwin, R.W., 1986. Endocytosis of a monoclonal antibody recognising a cell surface glycoprotein
544 antigen visualised using fluorescent conjugates. *Eur. J. Cell Biol.* 221, 214–221.

545 Gastaminza, P., Dryden, K.A., Boyd, B., Wood, M.R., Law, M., Yeager, M., Chisari, F. V., 2010. Ultrastructural
546 and Biophysical Characterization of Hepatitis C Virus Particles Produced in Cell Culture. *J. Virol.* 84, 10999–
547 11009. <https://doi.org/10.1128/jvi.00526-10>

548 Gaur, P.K., Mishra, S., Bajpai, M., Mishra, A., 2014. Enhanced oral bioavailability of Efavirenz by solid lipid
549 nanoparticles: In vitro drug release and pharmacokinetics studies. *Biomed Res. Int.* 2014.
550 <https://doi.org/10.1155/2014/363404>

551 Greve, J.M., Davis, G., Meyer, A.M., Forte, C.P., Yost, S.C., Marlor, C.W., Kamarck, M.E., McClelland, A., 1989.
552 The major human rhinovirus receptor is ICAM-1. *Cell* 56, 839–847. [https://doi.org/10.1016/0092-](https://doi.org/10.1016/0092-8674(89)90688-0)
553 [8674\(89\)90688-0](https://doi.org/10.1016/0092-8674(89)90688-0)

554 Grove, J., Marsh, M., 2011. The cell biology of receptor-mediated virus entry. *J. Cell Biol.* 195, 1071–1082.
555 <https://doi.org/10.1083/jcb.201108131>

556 Harvie, P., Désormeaux, A., Bergeron, M.C., Tremblay, M., Beauchamp, D., Poulin, L., Bergeron, M.G., 1996.
557 Comparative pharmacokinetics, distributions in tissue, and interactions with blood proteins of conventional

558 and sterically stabilized liposomes containing 2',3'-dideoxyinosine. *Antimicrob. Agents Chemother.* 40, 225–
559 229. <https://doi.org/10.1128/aac.40.1.225>

560 Henquell, C., Mirand, A., Deusebis, A.L., Regagnon, C., Archimbaud, C., Chambon, M., Bailly, J.L., Gourdon, F.,
561 Hermet, E., Dauphin, J.B., Labbé, A., Peigue-Lafeuille, H., 2012. Prospective genotyping of human
562 rhinoviruses in children and adults during the winter of 2009-2010. *J. Clin. Virol.* 53, 280–284.
563 <https://doi.org/10.1016/j.jcv.2011.10.009>

564 Hillaireau, H., Le Doan, T., Appel, M., Couvreur, P., 2006. Hybrid polymer nanocapsules enhance in vitro delivery
565 of azidothymidine-triphosphate to macrophages. *J. Control. Release* 116, 346–352.
566 <https://doi.org/10.1016/j.jconrel.2006.09.016>

567 Hofer, F., Gruenberger, M., Kowalski, H., Machat, H., Huettinger, M., Kuechler, E., Blaas, D., 1994. Members of
568 the low density lipoprotein receptor family mediate cell entry of a minor-group common cold virus. *Proc.*
569 *Natl. Acad. Sci. U. S. A.* 91, 1839–1842. <https://doi.org/10.1073/pnas.91.5.1839>

570 Irwin, K.K., Renzette, N., Kowalik, T.F., Jensen, J.D., 2016. Antiviral drug resistance as an adaptive process. *Virus*
571 *Evol.* 2, 1–10. <https://doi.org/10.1093/ve/vew014>

572 Johnston, S.L., Pattemore, P.K., Sanderson, G., Smith, S., Lampe, F., Josephs, L., Symington, P., Toole, S. o.,
573 Myint, S.H., Tyrrell, D.A.J., Holgate, S.T., 1995. Community study of role of viral infections in exacerbations
574 of asthma in 9-11 year old children. *Bmj* 310, 1225. <https://doi.org/10.1136/bmj.310.6989.1225>

575 Kallinteri, P., Higgins, S., Hutcheon, G.A., St. Pourçain, C.B., Garnett, M.C., 2005. Novel functionalized
576 biodegradable polymers for nanoparticle drug delivery systems. *Biomacromolecules* 6, 1885–1894.
577 <https://doi.org/10.1021/bm049200j>

578 Kiang, D., Yagi, S., Kantardjieff, K.A., Kim, E.J., Louie, J.K., Schnurr, D.P., 2007. Molecular characterization of a
579 variant rhinovirus from an outbreak associated with uncommonly high mortality. *J. Clin. Virol.* 38, 227–237.
580 <https://doi.org/10.1016/j.jcv.2006.12.016>

581 Lembo, D., Donalisio, M., Cibra, A., Argenziano, M., Cavalli, R., 2018. Nanomedicine formulations for the delivery
582 of antiviral drugs: a promising solution for the treatment of viral infections. *Expert Opin. Drug Deliv.* 15, 93–

583 114. <https://doi.org/10.1080/17425247.2017.1360863>

584 Lembo, D., Swaminathan, S., Donalisio, M., Civra, A., Pastero, L., Aquilano, D., Vavia, P., Trotta, F., Cavalli, R.,
585 2013. Encapsulation of Acyclovir in new carboxylated cyclodextrin-based nanosponges improves the agent's
586 antiviral efficacy. *Int. J. Pharm.* 443, 262–272. <https://doi.org/10.1016/j.ijpharm.2012.12.031>

587 Lindenbach, B.D.M.J.E., Syder, A.J., Wolk, B., Timothy L. Tellinghuisen, Christopher C. Liu, Toshiaki
588 Maruyama, R.O.H., Burton, D.R., McKeating, J.A., Rice, C.M., 2005. Replication of hepatitis C virus in cell
589 culture. *Science* (80-.). 309, 623–626. <https://doi.org/10.7124/bc.0007C9>

590 Mäkelä, M.J., Puhakka, T., Ruuskanen, O., Leinonen, M., Saikku, P., Kimpimäki, M., Blomqvist, S., Hyypiä, T.,
591 Arstila, P., 1998. Viruses and bacteria in the etiology of the common cold. *J. Clin. Microbiol.* 36, 539–542.
592 <https://doi.org/10.1128/jcm.36.2.539-542.1998>

593 Meng, W., Parker, T.L., Kallinteri, P., Walker, D.A., Higgins, S., Hutcheon, G.A., Garnett, M.C., 2006. Uptake and
594 metabolism of novel biodegradable poly (glycerol-adipate) nanoparticles in DAOY monolayer. *J. Control.*
595 *Release* 116, 314–321. <https://doi.org/10.1016/j.jconrel.2006.09.014>

596 Moyle, G., 2000. Clinical Manifestations and Management Nucleoside Analog-Related Mitochondrial Graeme
597 Moyle, MD, MBBS, Dip Genitourinary of Antiretroviral Toxicity Medicine. *Clin. Ther.* 22, 911–936.

598 Nicholson, K.G., Kent, J., Ireland, D.C., 1993. Respiratory viruses and exacerbations of asthma in adults. *Br. Med.*
599 *J.* 307, 982–986. <https://doi.org/10.1136/bmj.307.6910.982>

600 Nii-Trebi, N.I., 2017. Emerging and Neglected Infectious Diseases: Insights, Advances, and Challenges. *Biomed*
601 *Res. Int.* 2017. <https://doi.org/10.1155/2017/5245021>

602 Nowacek, A., 2010. NIH Public Access NanoART, neuroAIDS and CNS drug delivery. *Nanomedicine (Lond)* 4,
603 557–574. <https://doi.org/10.2217/nnm.09.38.NanoART>

604 Ochekepe, N.A., Olorunfemi, P.O., Ngwuluka, N.C., 2009. Nanotechnology and drug delivery part 1: Background
605 and applications. *Trop. J. Pharm. Res.* 8, 265–274. <https://doi.org/10.4314/tjpr.v8i3.44546>

606 Oventa, F.R.N., Tanzial, A.N.N.A.M.A.S., Olero, P.I.S., Orrocher, R.O.C., 2000. Hemolytic Anemia Induced by
607 Ribavirin Therapy in Patients With Chronic Hepatitis C Virus Infection : Role of Membrane Oxidative

608 Damage. *Hepatology* 31, 39–45. <https://doi.org/10.1053/he.2000.5789>

609 Papi, A., Bellettato, C.M., Braccioni, F., Romagnoli, M., Casolari, P., Caramori, G., Fabbri, L.M., Johnston, S.L.,
610 2006. Infections and airway inflammation in chronic obstructive pulmonary disease severe exacerbations. *Am.*
611 *J. Respir. Crit. Care Med.* 173, 1114–1121. <https://doi.org/10.1164/rccm.200506-859OC>

612 Peters, C.J., LeDuc, J.W., 1999. An Introduction to Ebola: The Virus and the Disease. *J. Infect. Dis.* 179, Six-xvi.
613 <https://doi.org/10.1086/514322>

614 Pileri, P., Uematsu, Y., Campagnoli, S., Galli, G., Falugi, F., Petracca, R., Weiner, A.J., Houghton, M., Rosa, D.,
615 Grandi, G., Abrignani, S., 1998. Binding of hepatitis C virus to CD81. *Science* (80-.). 282, 938–941.
616 <https://doi.org/10.1126/science.282.5390.938>

617 Pradhan, P., Pandey, A.K., Mishra, A., Gupta, P., Tripathi, P.K., Menon, M.B., Gomes, J., Vivekanandan, P.,
618 Kundu, B., 2020. Uncanny similarity of unique inserts in the 2019-nCoV spike protein to HIV-1 gp120 and
619 Gag. <https://doi.org/10.1101/2020.01.30.927871>.

620 Reddel, R.R., Ke, Y., Gerwin, B.I., McMenamin, M.G., Lechner, J.F., Su, R.T., Brash, D.E., Park, J.B., Rhim, J.S.,
621 Harris, C.C., 1988. Transformation of Human Bronchial Epithelial Cells by Infection with SV40 or
622 Adenovirus-12 SV40 Hybrid Virus, or Transfection via Strontium Phosphate Coprecipitation with a Plasmid
623 Containing SV40 Early Region Genes. *Cancer Res.* 48, 1904–1909.

624 Sayers, E.J., Peel, S.E., Schantz, A., England, R.M., Beano, M., Bates, S.M., Desai, A.S., Puri, S., Ashford, M.B.,
625 Jones, A.T., 2019. Endocytic Profiling of Cancer Cell Models Reveals Critical Factors Influencing LNP-
626 Mediated mRNA Delivery and Protein Expression. *Mol. Ther.* 27, 1–13.
627 <https://doi.org/10.1016/j.ymthe.2019.07.018>

628 Scarselli, E., Ansuini, H., Cerino, R., Roccasecca, R.M., Acali, S., Filocamo, G., Traboni, C., Nicosia, A., Cortese,
629 R., Vitelli, A., 2002. The human scavenger receptor class B type I is a novel candidate receptor for the
630 hepatitis C virus. *EMBO J.* 21, 5017–5025. <https://doi.org/10.1093/emboj/cdf529>

631 Schober, D., Kronenberger, P., Prchla, E., Blaas, D., Fuchs, R., 1998. Major and Minor Receptor Group Human
632 Rhinoviruses Penetrate from Endosomes by Different Mechanisms. *J. Virol.* 72, 1354–1364.

633 <https://doi.org/10.1128/jvi.72.2.1354-1364.1998>

634 Schuler, B.A., Schreiber, M.T., Li, L., Mokry, M., Kingdon, M.L., Raugi, D.N., Smith, C., Hameister, C.,
635 Racaniello, V.R., Hall, D.J., 2014. Major and Minor Group Rhinoviruses Elicit Differential Signaling and
636 Cytokine Responses as a Function of Receptor-Mediated Signal Transduction. *PLoS One* 9.
637 <https://doi.org/10.1371/journal.pone.0093897>

638 Shanks, G.D., Brundage, J.F., 2012. Pathogenic responses among young adults during the 1918 influenza pandemic.
639 *Emerg. Infect. Dis.* 18, 201–207. <https://doi.org/10.3201/eid1802.102042>

640 Soota, K., Maliakkal, B., 2014. Ribavirin induced hemolysis : A novel mechanism of action against chronic hepatitis
641 C virus infection. *World J. Gastroenterol.* 20, 16184–16190. <https://doi.org/10.3748/wjg.v20.i43.16184>

642 Stobart, C.C., Nosek, J.M., Moore, M.L., 2017. Rhinovirus biology, antigenic diversity, and advancements in the
643 design of a human rhinovirus vaccine. *Front. Microbiol.* 8, 1–8. <https://doi.org/10.3389/fmicb.2017.02412>

644 Szunerits, S., Barras, A., Khanal, M., Pagneux, Q., Boukherroub, R., 2015. Nanostructures for the inhibition of viral
645 infections. *Molecules* 20, 14051–14081. <https://doi.org/10.3390/molecules200814051>

646 Winther, B., 2011. Rhinovirus infections in the upper airway. *Proc. Am. Thorac. Soc.* 8, 79–89.
647 <https://doi.org/10.1513/pats.201006-039RN>

648 Zhang, C., Zheng, W., Huang, X., Bell, E.W., Zhou, X., Zhang, Y., 2020. Protein structure and sequence re-analysis
649 of 2019-nCoV genome does not indicate snakes as its intermediate host or the unique similarity between its
650 spike protein insertions and HIV-1 2.

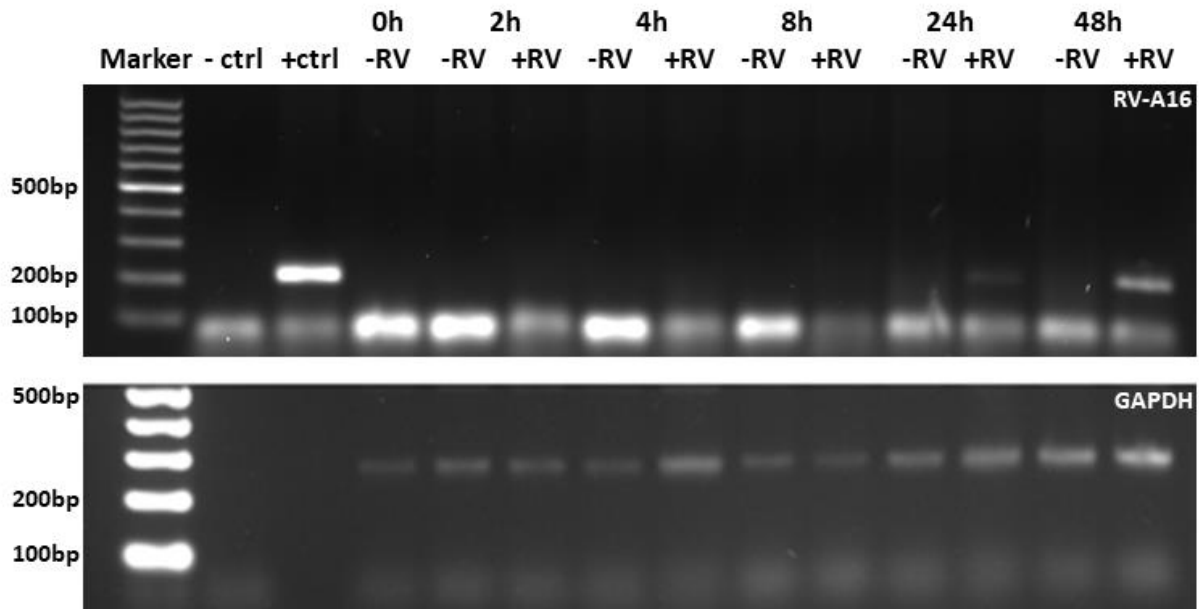
651 Zhang, T., Howell, B.A., Dumitrascu, A., Martin, S.J., Smith, P.B., 2014. Synthesis and characterization of glycerol-
652 adipic acid hyperbranched polyesters. *Polymer (Guildf).* 55, 5065–5072.
653 <https://doi.org/10.1016/j.polymer.2014.08.036>

654

655

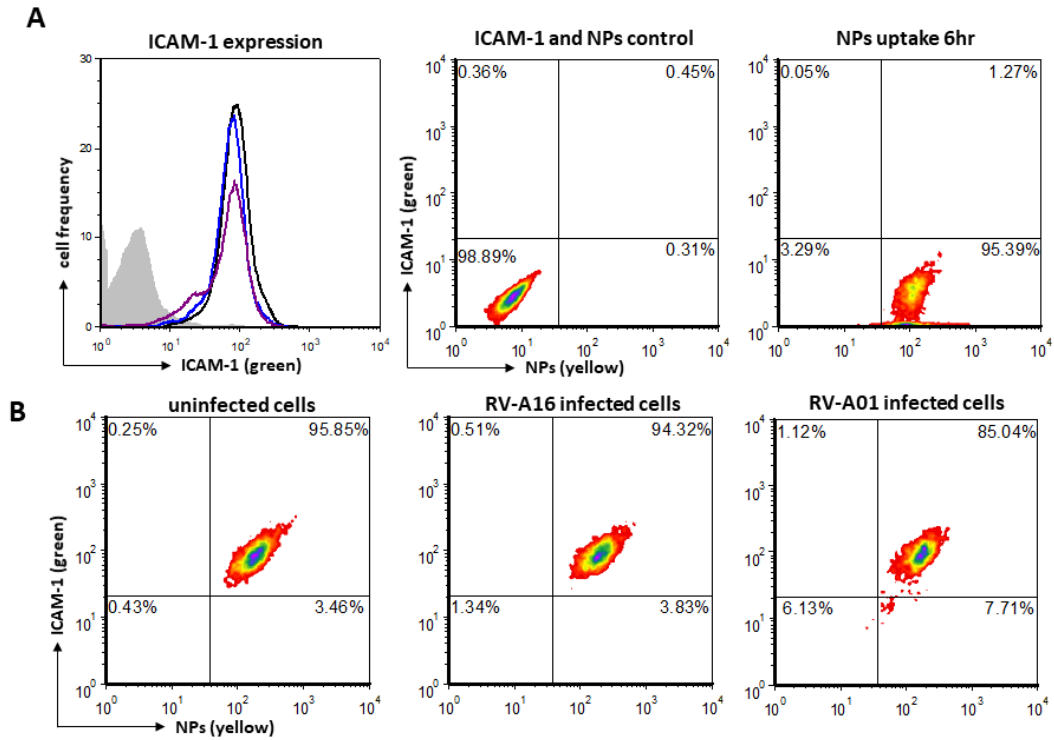
656

657 **Figures**



658

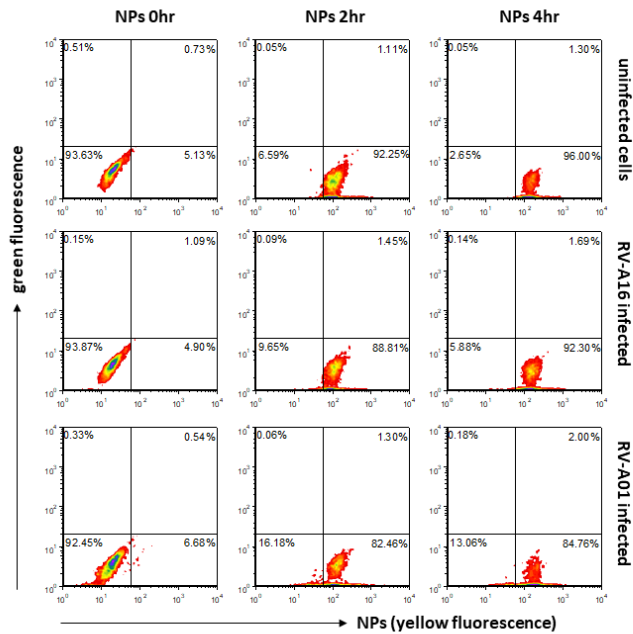
659 **Figure 1:** RV-A16 genome is detected 24 and 48 hours after infection. RT-PCR was performed
660 on RNA obtained from HeLa cells at the indicated timepoints and conditions (upper panel). -RV
661 refers to uninfected cells and +RV to cells infected with RV-A16 at MOI 0.5. Controls used were
662 cDNA of the RV16 genome (+ctrl) or dH₂O (-ctrl). The lower panel displays the same samples
663 where housekeeping gene GAPDH was amplified to demonstrate total RNA was present in each
664 sample.



665

666 **Figure 2:** Flow cytometry analysis of HeLa cells and NPs uptake. (A) ICAM-1 expression of
 667 uninfected cells (black line), RV-A16 infected (blue line) and RV-A01 infected (purple line)
 668 compared to unstained control cells (grey filled). Contour plots are shown demonstrating NPs
 669 uptake (yellow fluorescence) in the absence of ICAM-1 staining. (B) NPs uptake (yellow
 670 fluorescence) of uninfected and RV-A16 or RV-A01 infected cells co-stained with ICAM-1 (green
 671 fluorescence). Numbers represent % of gated cells within each quadrant.

672

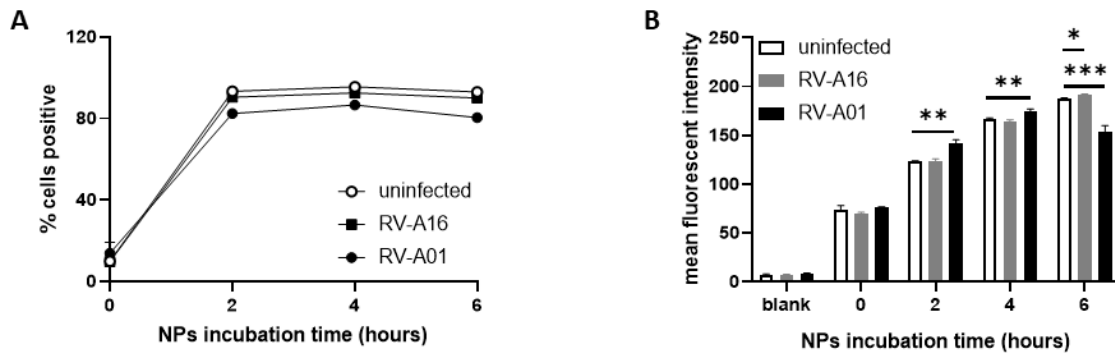


	NPs 0hr	NPs 2hr	NPs 4hr
uninfected	LL: 2189 LR: 120	LL: 131 LR: 1834	LL: 55 LR: 1993
RV-A16 infected	LL: 2586 LR: 135	LL: 207 LR: 1905	LL: 129 LR: 2025
RV-A01 infected	LL: 1702 LR: 123	LL: 274 LR: 1396	LL: 222 LR: 1441

673

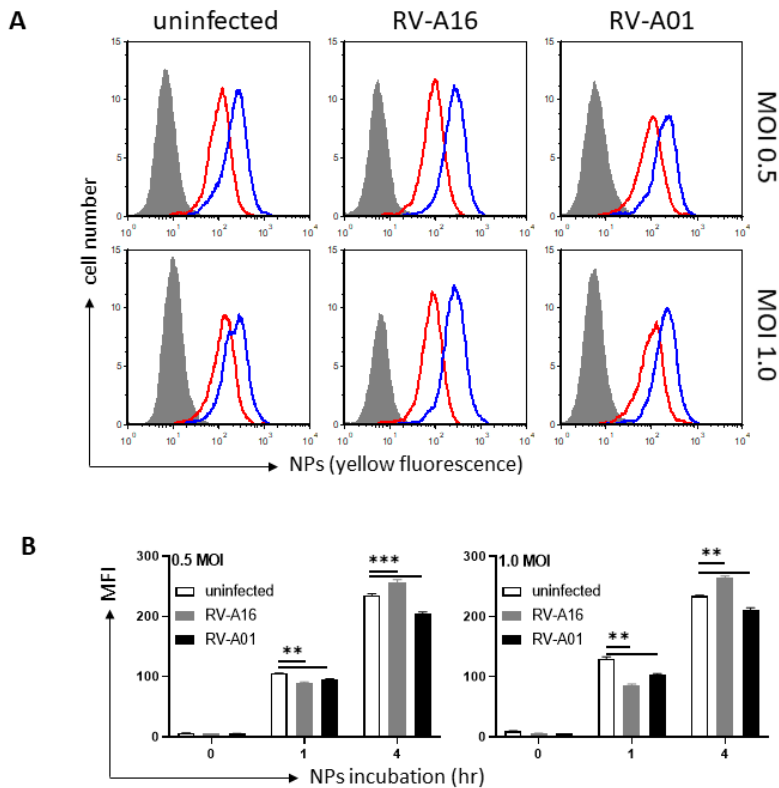
674 **Figure 3:** Time course analysis of NPs uptake by HeLa cells. Contour plots display NPs uptake
 675 (yellow fluorescence) of uninfected cells, RV-A16 infected cells, and RV-A01 infected cells at
 676 baseline (0hr) and for 2hr and 4hr. Numbers within contour plots represent % of gated cells within
 677 each quadrant. Numbers in the table represent quantitative cell numbers within lower left (LL) and
 678 lower right (LR) quadrants.

679



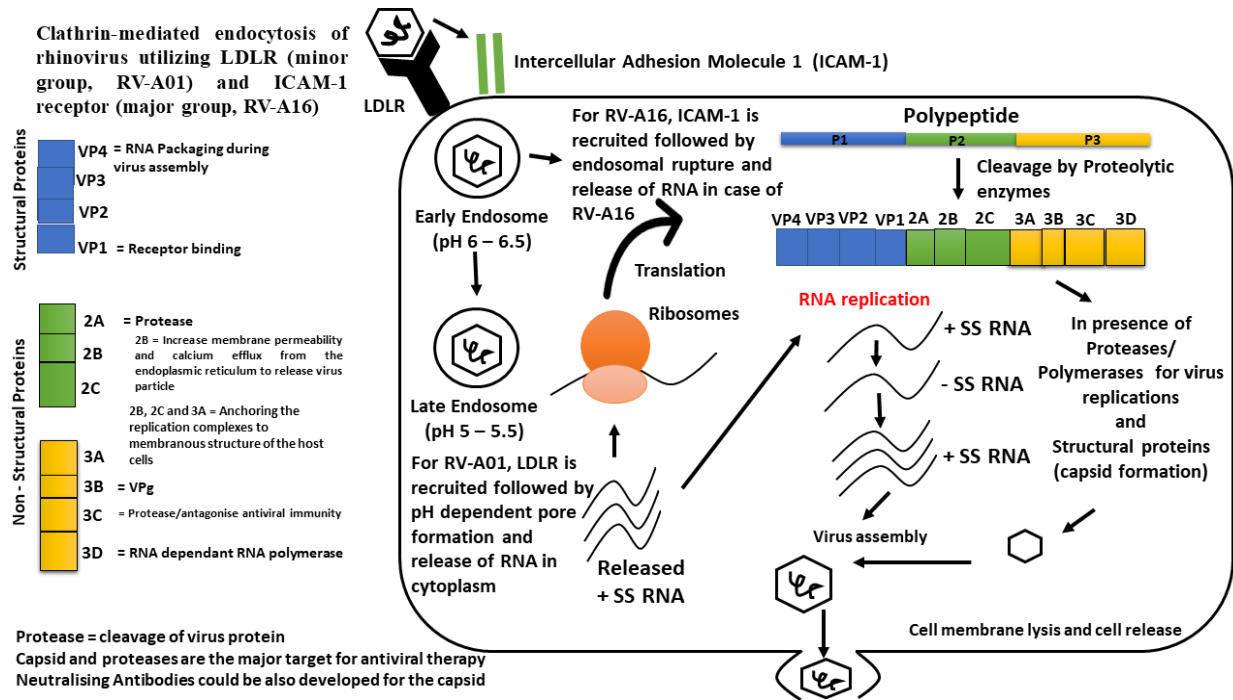
680

681 **Figure 4:** Time course analysis of NPs uptake by HeLa cells. (A) Data obtained from flow
 682 cytometry contour plots display NPs uptake as the percentage of fluorescent positive cells for
 683 uninfected cells (open circle), RV-A16 infected cells (closed square), and RV-A01 infected cells
 684 (closed circle) at the indicated timepoints. (B) NPs uptake data were analysed as mean fluorescent
 685 intensity of fluorescent positive cells for uninfected cells (white), RV-A16 infected cells (grey),
 686 and RV-A01 infected cells (black) at the indicated timepoints. Data were analysed by 2-way
 687 ANOVA and significant differences are denoted with asterisks (* $p < 0.05$; ** $p < 0.01$; ***
 688 $p < 0.001$).



689

690 **Figure 5:** Flow cytometry analysis of Beas2B cells and NPs uptake. (A) NPs uptake (yellow
 691 fluorescence) histograms of uninfected cells, RV-A16 infected and RV-A01 infected cells after
 692 1hr (red line) and 4hr (blue line) compared to control cells without NPs (grey filled). Two different
 693 MOI were used (0.5 and 1.0). (B) NPs uptake data were analysed as mean fluorescent intensity
 694 (MFI) of fluorescence for uninfected cells (white), RV-A16 infected cells (grey), and RV-A01
 695 infected cells (black) at the indicated timepoints and MOI. Data were analysed by 2-way ANOVA
 696 and significant differences are denoted with asterisks (** $p < 0.01$; *** $p < 0.001$).



697

698 **Figure 6:** Mechanism of RVs entry into cells.